Acta Cryst. (1968). A.24, 339

Observation of the Breakdown of Friedel's Law in Electron Diffraction and Symmetry Determination from Zero-Layer Interactions

BY P. GOODMAN

Division of Chemical Physics, Commonwealth Scientific and Industrial Research Organization, Melbourne, Australia

AND G. LEHMPFUHL

Fritz-Haber-Institut der Max-Planck-Gesellschaft, Berlin-Dahlem, Germany

(*Received* 25 *April* 1967 *and in revised form* 29 *July* 1967)

Detailed observations are made of the breakdown of Friedel's law in electron diffraction, using the single-crystal intensity distribution from cadmium sulphide in the [21$\bar{3}$0] orientation. It has been found by experiment that no breakdown of Friedel's law occurs in the zero-order beam distribution. An analysis of the problem due to Moodie, using multiple-scattering diagrams, has also led to this result. Multiple-scattering diagrams are used here to illustrate the symmetry properties of the zero-beam distribution. Rules are given for the deduction of the other symmetry elements of the projected structure from the diffraction-pattern symmetry, and from the occurrence of dynamic extinction bands in the kinematically forbidden reflexions. These are illustrated by further pictures from cadmium sulphide. This analysis is simplified in the present work by neglecting non-zero-layer interactions. Results obtained by *n*-beam calculation using the multi-slice method show the possibility of quantitative interpretation, and of absolute orientation determination. The limitations of the systematic dynamic approximation and also of a systematic approximation using corrected scattering potentials are examined for this substance.

1. Introduction

One of the deductions to be made from *n*-beam dynamic theory of electron diffraction is that Friedel's law should no longer hold for diffraction from a non-centrosymmetric structure. This is an example of a general property of dynamic intensities, namely their sensitivity to the phases of the structure factors and hence to the symmetry elements of the space group. However the element of centrosymmetry is in a class apart, since it cannot be detected directly in structure analysis based on the kinematic scattering theory of electrons, or the kinematic theory derived without absorption for X-rays (Friedel, 1913; von Laue, 1948). This and symmetries generated by reflexion operations are made obvious in the convergent beam electron diffraction pattern. If the dynamic intensities are expressed as a Born series (*e.g.* Cowley & Moodie, 1957; Fujiwara, 1959) it is seen that terms of second and higher order processes can lead to asymmetry in the diffraction pattern, and these terms can further be used for a more detailed analysis.

Asymmetry in diffraction from a non-centred structure was first reported by Thiessen & Molière (1939), who measured the mean inner potential by reflexion from the (111) and ($\bar{1}\bar{1}\bar{1}$) faces of zinc sulphide. Miyake & Uyeda (1950) observed asymmetry within the reflexion (Bragg case) diffraction pattern from zinc sulphide, in an experiment which eliminated trivial geometrical (excitation error) asymmetries. More recently Tanaka & Honjo (1964) have observed contrast between 180° domains in the bright-field images of barium titanate crystals, which they attribute to the failure of Friedel's law.

Ibers & Hoerni (1954) noted that complex scattering factors, first proposed as a correction to the kinematical theory, would lead to asymmetric intensities from a non-centred structure. Kohra (1954) independently pointed out that dynamic scattering without absorption processes could lead to this result, in violation of Friedel's law, at least in the Bragg case. By solving the 3-beam equations for the case of specular reflexion he obtained a numerical result which approximately fitted Miyake & Uyeda's observation, and subsequently these authors (Miyake & Uyeda, 1955) reconsidered the problem in detail. A more general deduction of the diffraction asymmetry from *n*-beam dynamic theory was made by Cowley & Moodie (1959), who derived the phase-grating approximation, and Fujimoto (1959) using a thickness expansion. The phase-grating formulation, which is the high-voltage limit of the dynamic theory, has the advantage of showing the character of the asymmetry as an oscillating function of thickness (Fig. 9).

The generation of dynamically forbidden regions in the kinematically forbidden intensities when certain symmetry elements are present was discussed by Cowley & Moodie (1959) and Cowley, Moodie, Miyake, Takagi & Fujimoto (1960). Recently a detailed interpretation of these absences was given by Gjønnes & Moodie (1965). As a consequence these regions may be used in symmetry analysis, without independent knowledge of the structure, giving a technique analogous to the X-ray method of observing kinematic absences. Analyses of the type demonstrated by Kambe (1957*a*,*b*), which determine the relative phases of specific structure factors from the dynamic intensities, are then logically a further stage in structure determina-

tion, rather than a direct examination of the symmetries.

Differences in the intensity distribution of symmetrically related diffracted beams from cadmium sulphide in transmission (Laue case) have recently been reported by Goodman & Lehmpfuhl (1964), from initial experiments using convergent beam technique. Extinction bands were observed on the kinematically forbidden 000*l* intensity distributions, along the [000*l*]* axis, and at right angles along the line of Bragg excitation. The present report gives a more detailed analysis of the cadmium sulphide pattern, in which *n*-beam calculations are used to obtain a quantitative interpretation of the pattern in the direction of the asymmetry. (The notation [ ]* has been adopted here to denote directions in reciprocal space, analogous to [ ] used for real space.)

The CdS patterns are used as an illustration for the general problem. It is shown that the symmetry of the diffraction pattern together with an identification of dynamic extinction bands determines the symmetry group of the projected structure, for the common case where higher layer interactions may be neglected. The numerical calculations serve to show the limitations of the systematic approximation in the case of heavier atoms and more complex structures, and the possibility of using other approximate methods of calculation is examined.

2. Observation of asymmetry

Friedel's law was originally formulated for X-ray diffraction (Friedel, 1913), but since that time has been applied in discussion to electron diffraction (*e.g.* von Laue, 1948). For electron diffraction we can define the law as:

$$(I_{hkl})^{uvw} = (I_{\bar{h}\bar{k}\bar{l}})^{\bar{u}\bar{v}\bar{w}}, \qquad (1)$$

representing the dynamic intensities corresponding to the incident beam directions (*uvw*), where u,v,w, are coordinates not necessarily integral. From dynamic diffraction theory this law is expected to break down for non-centred structures; equation (1) then becomes the general condition for the existence of a centre of symmetry.

Testing the law rigorously involves comparing the diffraction pattern from the same crystal at two settings, the second setting being obtained by a 180° rotation perpendicular to the incident direction. However, it is more valuable to discuss the symmetries expected from a single (zone axis) setting. From the form of the *n*-beam solution as a sum of terms containing products of the kinematic structure factors, F_{hkl}, elementary rules may be deduced. The symmetries of the structure are introduced differently by the zero and upper layers, so that the latter need to be considered separately. However, the upper layers may introduce asymmetry into an otherwise symmetrical zero-layer pattern, but not the reverse. Therefore a centrosymmetric convergent beam pattern or group of patterns defined by

$$(I_{hk0})^{uvw} = (I_{\bar{h}\bar{k}0})^{\bar{u}\bar{v}w} \qquad (2)$$

for the [001] projection, may be interpreted as arising from a structure which is at least centred in that projection. The asymmetric pattern has no such direct interpretation, but provided certain other conditions are known to hold, namely,

$$F_{hkl} = \pm F_{hk\bar{l}} \qquad (3)$$

for all possible reflexions, it will be proof of the *lack* of a centre in the projection, and therefore in the structure as a whole. The investigation may be usefully carried out for any direction of relatively low index in the crystal. In this case re-indexing the crystal so that $l=0$ for the zero layer makes relations (2) and (3) applicable to any zone axis pattern. Relation (3) is the condition for finding in the structure a mirror or glide plane perpendicular to [001]. For all other conditions the higher-layer interactions may themselves introduce observable non-centrosymmetry.

Projected structure

Since in many cases the projected structure alone is sufficient to explain the main features of a zone-axis pattern, it is useful to consider the two-dimensional structure, and its associated diffraction pattern containing zero-layer reflexions only, as a special case. With this simplification the centrosymmetry of the projection is directly displayed by the pattern. In addition a pattern may have one or more lines of reflexion, along principal axes. The diffraction pattern will have a mirror line [0*k*]* if the relation,

$$F_{hk} = \pm F_{\bar{h}k} \qquad (4)$$

holds with either sign (+) and (−) corresponding to a mirror line or glide ($b/2$) line in the structure respectively. However, the latter condition is distinguished by kinematically forbidden reflexions, defined by ($h=0$; $k=2n+1$), for which the dynamic intensity goes to zero along the [0*k*]* axis (Gjønnes & Moodie, 1965). A recognition of this characteristic zero-band in alternative {0*k*} reflexions therefore enables the diffraction pattern symmetry to be fully analysed.† Illustrations of these two possibilities are provided by the [000*l*]* axis, indicated in the two diffraction patterns of Figs. 2 and 3 (see § 4).

† Apart from the reservation that upper-layer line interactions are ignored, this analysis refers only to the symmetry elements of the projection. As pointed out by Cowley, Moodie, Miyake, Takagi & Fujimoto (1961), certain three-dimensional space-group-forbidden reflexions after projection are degraded into 'accidental'-forbidden reflexions, which will *not* be dynamically forbidden on the axis. Therefore such elements as 3-, 4- and 6-fold screw axes cannot be deduced from the diffraction pattern of the zone. However, by turning the crystal so as to excite only the on-axis reflexions, thus destroying the dynamic paths of the forbidden reflexions, the intensities of the latter will go to zero, giving the additional information necessary for the deduction of these elements.

Two of either glide- or mirror-reflexion lines at right-angles will ensure also a centre of symmetry (*e.g. pmm*, *pgg*, *pmg*); alternatively, a centre of symmetry may exist without any reflexion lines.

3. Symmetry of the zero beam distribution

In electron diffraction we may measure the zero (direct transmitted) beam intensity. This beam is unique in the dynamic scattering problem owing to the boundary condition that it alone has intensity at the entrance face. By analysis of terms from the general series, in the manner of Gjønnes & Moodie, Moodie (1968) has shown that this condition imposes a higher degree of symmetry on the zero beam distribution than for the other beams.

The proof of the relation

$$(I_{000})^{uvw}=(I_{000})^{\bar{u}\bar{v}\bar{w}} \tag{5}$$

for all structures means effectively that Friedel's law holds unconditionally for the zero-beam distribution, even when it breaks down for the other beams† (as in the case of a non-centred structure).

To consider, as was done for the diffracted beams in § 2, the symmetry of a single zero-beam pattern about a principle direction, it follows that when the conditions described by relation (3) exist, this pattern must be centrosymmetric, even with a non-centrosymmetric structure. This central beam symmetry was first detected experimentally in a group of symmetrically disposed convergent beam patterns taken about the [21$\bar{3}$0] axis of cadmium sulphide (Fig. 4) (see § 4).

The symmetries of the zero-beam distribution may be analysed by use of the multiple-scattering diagrams described by Gjønnes & Moodie (1965). Following Moodie (1968), the zero-order amplitude may be expressed in terms of paired, closed-loop processes (Fig. 6), as for example a third-order process

$$\underset{(1)}{[(F_{h1}F_{h2}F_{\bar{h}3})}+\underset{(2)}{(F_{h3}F_{\bar{h}2}F_{\bar{h}1})}]\,.\,Z(\zeta) \tag{6a}$$

(see Fig. 6), where $(F_{h1}\ \ldots)$ *etc.* are products of structure factors, and the $Z(\zeta)$ are the homogeneous functions of the excitation errors defined by Cowley & Moodie (1962). The invariance of such expressions to inversion through the origin, establishes the generality of relation (5).

Projected structure

If we now as in § 2 treat the two-dimensional problem as a special case, ignoring upper-layer effects, corresponding and equal expressions to (6*a*), namely

$$\underset{(3)}{[(F_{\bar{h}1}F_{\bar{h}2}F_{h3})}+\underset{(4)}{(F_{\bar{h}3}F_{h2}F_{h1})}]\,.\,Z(\zeta) \tag{6b}$$

† J. Cowley, A. Pogany and P. Turner have pointed out that the symmetry property of the zero beam referred to is a direct consequence of the theorem of reciprocity, first enunciated by von Laue. Implications of this theorem are discussed in a work to be published by these authors.

(see Fig. 6) may always be found on the opposite side of the zone axis, demonstrating that at least a centre of symmetry must exist in the zero pattern under these conditions, when the rest of the diffraction pattern has none. Other equivalent pairs, depicted by (*e*) and (*f*) in Fig. 6, may be found, depending upon axes of symmetry occurring in the projected structure, resulting in fourfold, sixfold, *etc.* symmetry in the zero beam pattern. Thus it may be deduced from expressions of the form of (6) above, that reflexion symmetry will exist in the zero-pattern across an axis $[0k]^*$ if either of the relations,

$$F_{hk}=\pm F_{\bar{h}k}\,,$$
$$F_{hk}=\pm F^*_{\bar{h}k}\,,$$

holds, or in other words if

$$|F_{hk}|=|F_{\bar{h}k}|\,. \tag{7}$$

For reflexion symmetry to be generated in the diffraction pattern, the more restrictive relation (4) must hold. Therefore a reflexion line may exist in the zero-beam distribution which is not a reflexion line in the diffraction pattern. (Example Fig. 2: $[h,2\bar{h},h,0]^*$ axis.) This proof could be extended to show that when upper-layer terms are included provided relation (3) holds, these rules are still valid.

The simple relations (4) and (7) are not the general conditions for symmetrical intensity; however the influence of upper layers is in many cases very weak, so that they should be useful, at least initially, in analysis. A fuller discussion considering the three-dimensional symmetry properties will be given elsewhere.

Upper layers

According to (7) the zero pattern is always centric, so that this property gives no structural information, but serves experimentally as a marker (see § 4). In fact no unique structural information is obtained from this distribution if we have only zero-layer interaction; its value lies in its ability to reveal upper-layer effects where these are likely to destroy symmetries in the diffraction pattern. This allows a practical approach. We cannot know in commencing an analysis if the symmetries of relation (3) exist, but the zero pattern shows the practical point, *i.e.* when their non-existence is of importance.

A symmetric zero pattern allows one to interpret an asymmetric diffraction pattern in terms of an asymmetric projected structure. This is the case in the analyses from Figs. 2, 4 and 5; the lack of centre is determined from a single pattern, since a non-centric diffraction pattern occurs together with a centric zero pattern. Conversely, a non-centric zero pattern indicates the influence of upper layers together with the absence of glide or mirror planes perpendicular to the projection, so that asymmetry in the pattern cannot be interpreted uniquely. Where a pattern is obtained showing non-centric distributions both in the zero beam and the diffraction pattern so that the two effects (*i.e.*

upper layers and lack of centre) cannot be separated, a second pattern should be taken with the crystal rotated 180° with respect to the first, and a reversal of pattern asymmetry will then indicate non-centrosymmetry in the structure.

Directions of projections used in the present investigation, namely [10$\bar{1}$0], [21$\bar{3}$0], and [32$\bar{5}$0], are shown on a diagram of the cadmium sulphide structure projected in the [0001] direction in Fig. 1. Here it is seen that the first two projections satisfy the conditions given by the relation (3). Therefore, knowing the structure, it is seen that the two pattern symmetries analysed in the next section refer directly to the projected symmetries, even in the presence of higher-layer interactions. In the case of the [32$\bar{5}$0] projection the relations (4) are not satisfied, and some higher-layer lines asymmetric about the horizontal axis of the picture may be seen in the outer regions of Fig. 7(*c*), although their influence on the intensities measured is extremely weak. Correspondingly, no attempt has been made in the calculations discussed in § 5 to introduce correctly the interaction of higher-layer reflexions.

4. Experimental method; results from zone-axis orientation

Thin cadmium sulphide plates (500–1500 Å) having (10$\bar{1}$0) principal faces were found in samples grown from the vapour phase.† These crystals were examined by convergent beam diffraction, at first in a Siemens Elmiskop I using a back-focal-plane heating stage described previously (Goodman & Lehmpfuhl, 1965) (Figs. 3 and 4) and later in a special diffraction apparatus (Cockayne, Goodman, Mills & Moodie, 1967) (Figs. 2, 5 and 7).

Fig. 2 shows the diffraction pattern with the incident beam cone symmetrical about the [21$\bar{3}$0] direction, and a diagrammatic representation of the structure projected in that direction (inset). The pattern shows complete symmetry across the [000*l*]* axis, the details in each $h\bar{2}hhl$ diffraction distribution being exactly reflected in the $\bar{h}2\bar{h}hl$ distribution. However no mirror line exists perpendicular to this axis: the reflexions $\bar{h}2hhl$, $h2\bar{h}\bar{h}l$ form no pairs. Thus the diffraction pattern symmetry reflects precisely the symmetry of the projected structure.

In Fig. 4 the incident beam has been moved so as to be at equal inclinations on either side of the zone axis [Fig. 4(*a*) and (*c*)], and exactly down the zone axis [Fig. 4(*b*)]. Here it is remarkable that the intensity distribution exactly repeats in the zero beam for equal angles of tilt, whereas the diffracted beams form no companion pairs in the two pictures. This observation is in agreement with Moodie's (1968) deduction from the theory. The uniqueness of the zero beam in this respect gives us a valuable experimental aid. Points recognized as equivalent in the zero beam patterns of such a pair of pictures can be taken as markers, to aid in the detection of quite small asymmetries in the diffracted distributions. It can be seen that cadmium sulphide has a gross asymmetry compared with the sensitivity of the method.

Extending this experimentally, Fig. 5 shows a set of four pictures taken with the zero beam on the corners of a rectangle in reciprocal space, symmetrical about the zone axis. Here we see that the zero-beam intensity distribution has two mirror lines, given by the two crystallographic axes, whereas the diffracted beam distributions have only one mirror line, *i.e.* about the [000*l*]* axis. The observation is extended to tilts from the zone axis of $\pm 1{\cdot}7°$ and $\pm 0{\cdot}7°$ as compared with approximately $\pm 0{\cdot}3°$ covered in the single observation (Fig. 2). Such an extension, as in Figs. 4 and 5, may

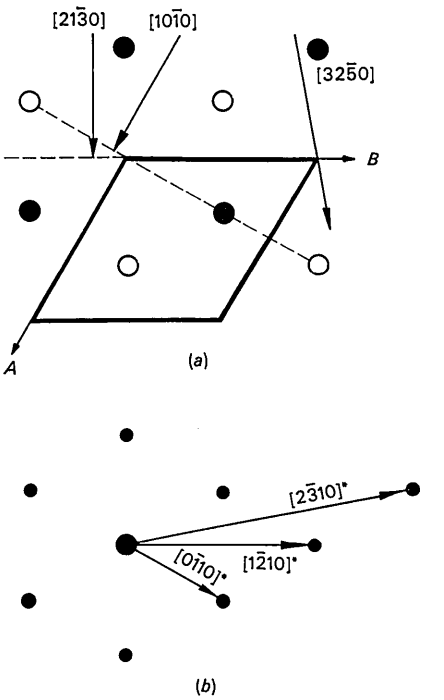

Fig. 1. (*a*) [0001] projection of cadmium sulphide. Atomic positions marked are for superimposed Cd+S; full and open circles represent these atoms at $z=0,\frac{1}{2}$, respectively. Boundary of a single unit cell is shown, enclosing a unit maximum symmetry. The three projections referred to in the text are indicated. Broken lines perpendicular to these directions represent planes of symmetry which for [10$\bar{1}$0] and [21$\bar{3}$0] vectors are mirror and glide (*c*/2) planes respectively. For the [32$\bar{5}$0] vector no perpendicular mirror or glide plane exists. Consequently relation (3) of the text holds for the first two projections only. (*b*) The reciprocal lattice section, $l=0$, showing reflexion vectors occurring in the patterns of Figs. 2, 3 & 7, which are taken from the projections shown in (*a*). The reciprocal lattice geometry is symmetrical about the [0$\bar{1}$10]* and [1$\bar{2}$10]* vectors. Consequently there is a *possibility* for the relation (3) of the text to hold for the corresponding (*viz.* [10$\bar{1}$0] and [21$\bar{3}$0]) projections. However, the geometry is unsymmetrical about the [2$\bar{3}$10]* vector, so that the relation cannot hold for the [32$\bar{5}$0] projection.

† Cadmium sulphide crystals were kindly supplied by Frau Dr Broser of Fritz-Haber-Institut, Berlin.

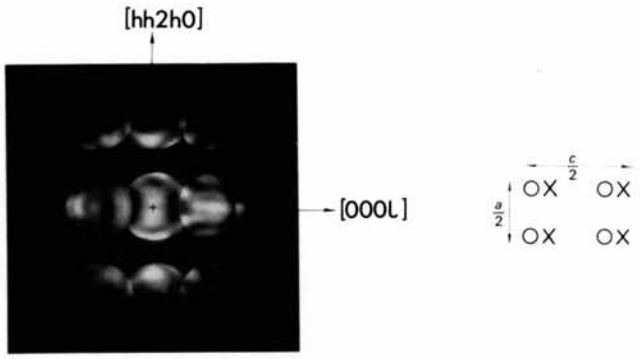

Fig. 2. Convergent beam diffraction pattern from the [21$\bar{3}$0] projection of cadmium sulphide. The cross (+) marks the zone axis, in the 0000 beam distribution. The diffraction pattern shows mirror symmetry about the [0001]* (horizontal) axis only. The central beam distribution shows an additional mirror symmetry. The inset shows the projected structure (*pm* symmetry), corresponding to orientation of the pattern.

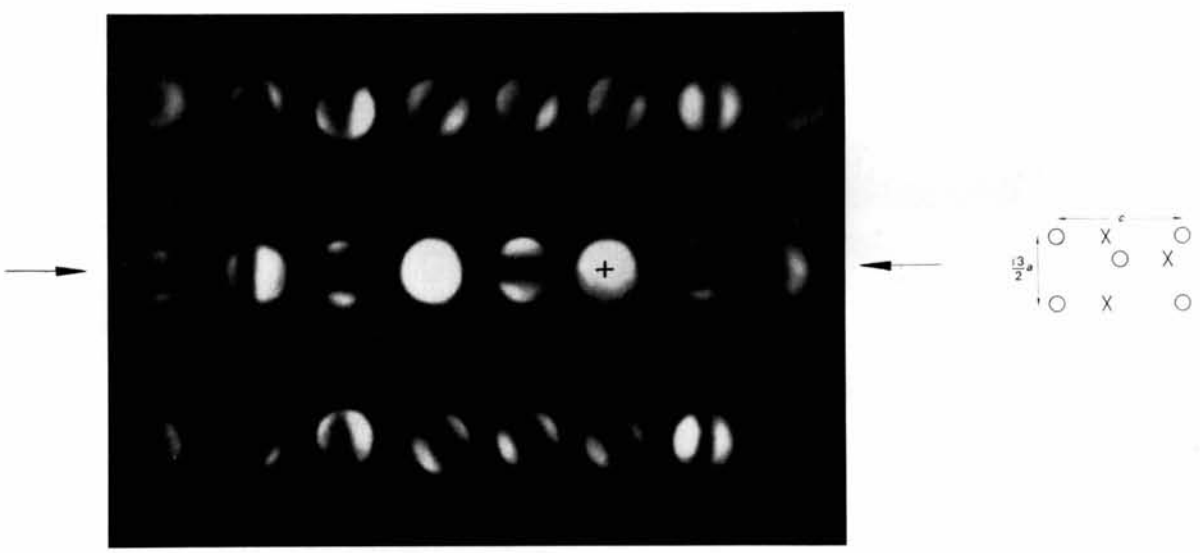

Fig. 3. Convergent beam pattern near the [10$\bar{1}$0] zone-axis of cadmium sulphide. The incident beam is symmetrically aligned with respect to the [000*l*]* axis (indicated by arrows), and the zero-beam distribution is marked by a cross. Alternate spots on this line, which are the kinematically forbidden 000*l* reflexions, show the characteristic horizontal black band, generated by the glide-line symmetry of the planar group *pg*. As in Fig. 2 the pattern has symmetry across the [000*l*]* line (the lack of symmetry in the [000*l*]* direction here is due to the missetting off the zone-axis in this direction. The inset shows the projected structure for this orientation. Width of horizontal forbidden bands is ~4′ of arc; for the purpose of this illustration, however, the contrast has been greatly increased, so that the actual width appearing in the weaker spots is not significant (photograph: unheated backfocal plane stage in Siemens Elmiskop).

[*To face p.* 342

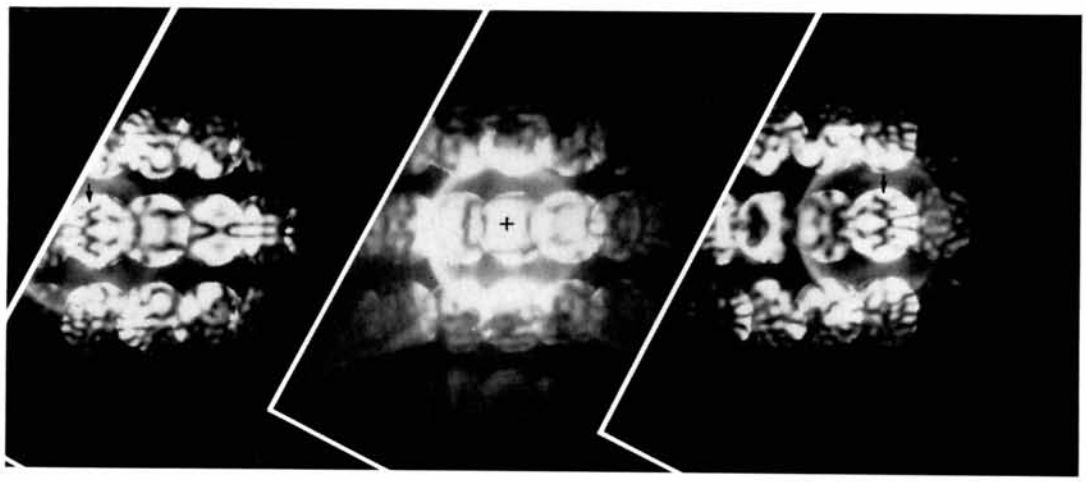

(*a*) (*b*) (*c*)

Fig. 4. Convergent beam patterns about the [21$\bar{3}$0] zone axis of cadmium sulphide: (*a*), (*c*), tilted equal amounts to either side of the axis (*i.e.* *hkl*; *hk*$\bar{l}$); (*b*) zone-axis orientation. Central beam patterns in (*a*) and (*c*) (indicated by arrows) are mirror images and are also centrosymmetric with respect to the zone axis [+ in (*b*)], but other diffraction distributions show no such symmetrical relationship, indicating the absence of mirror or glide reflexion symmetry in this (*i.e.* the [0001]) direction, and absence of the centre of symmetry in the projected structure.

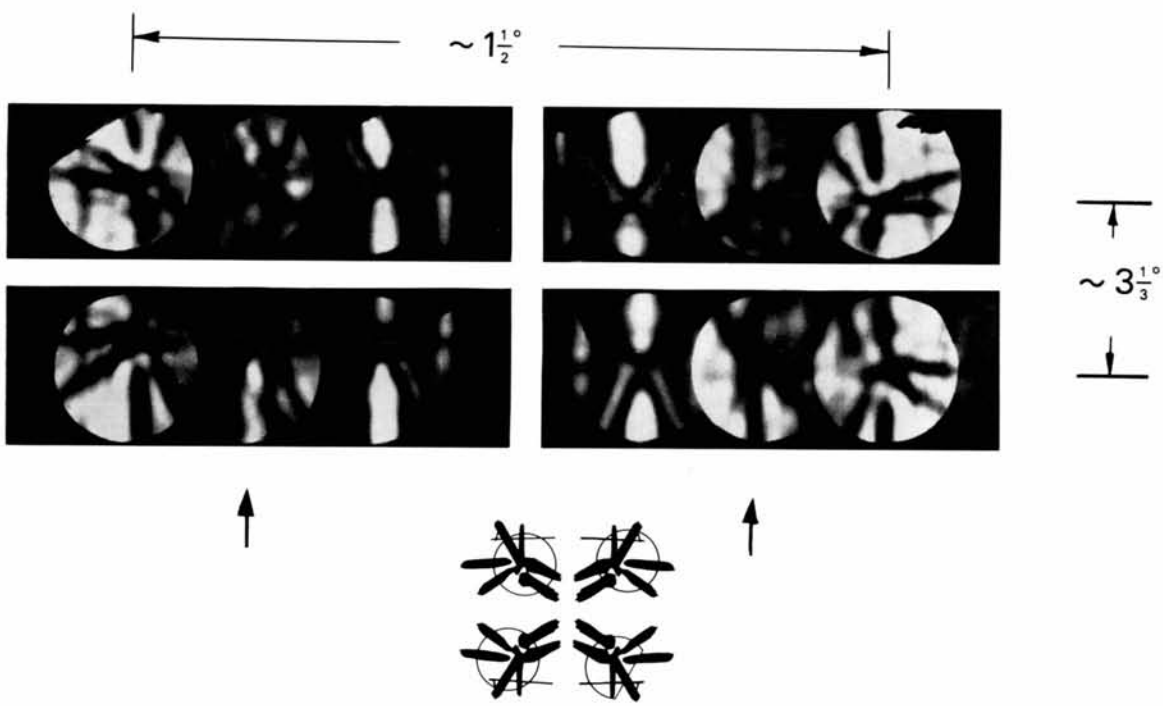

Fig. 5. Extension of experiment of Fig. 4. Incident beam inclined at four symmetrical tilts to the [21$\bar{3}$0] zone axis (*i.e.* defined by *hkl*, *hk*$\bar{l}$, $\bar{h}\bar{k}l$, $\bar{h}\bar{k}\bar{l}$). The central beam distribution which shows reflexion symmetry with respect to the two principal axes in the projection was used as a marker to locate the orientations. These were such as to excite the 0004, (000$\bar{4}$) and 2$\bar{4}$20, ($\bar{2}$4$\bar{2}$0) reflexions simultaneously; the rotation angles between settings are shown beside the Figure. The aperture is not exactly centred on the orientations but the inset shows the relative location of the same geometric pattern for the zero beam in the pictures (found in the four corners of the Figure), with respect to the aperture. The group of diffraction patterns shows reflexion symmetry about the horizontal but not the vertical axis. Indicated by an arrow-head, the 0002 distribution shows almost a black to white transformation in going from left to right picture, though no such change is found going from lower to upper picture.

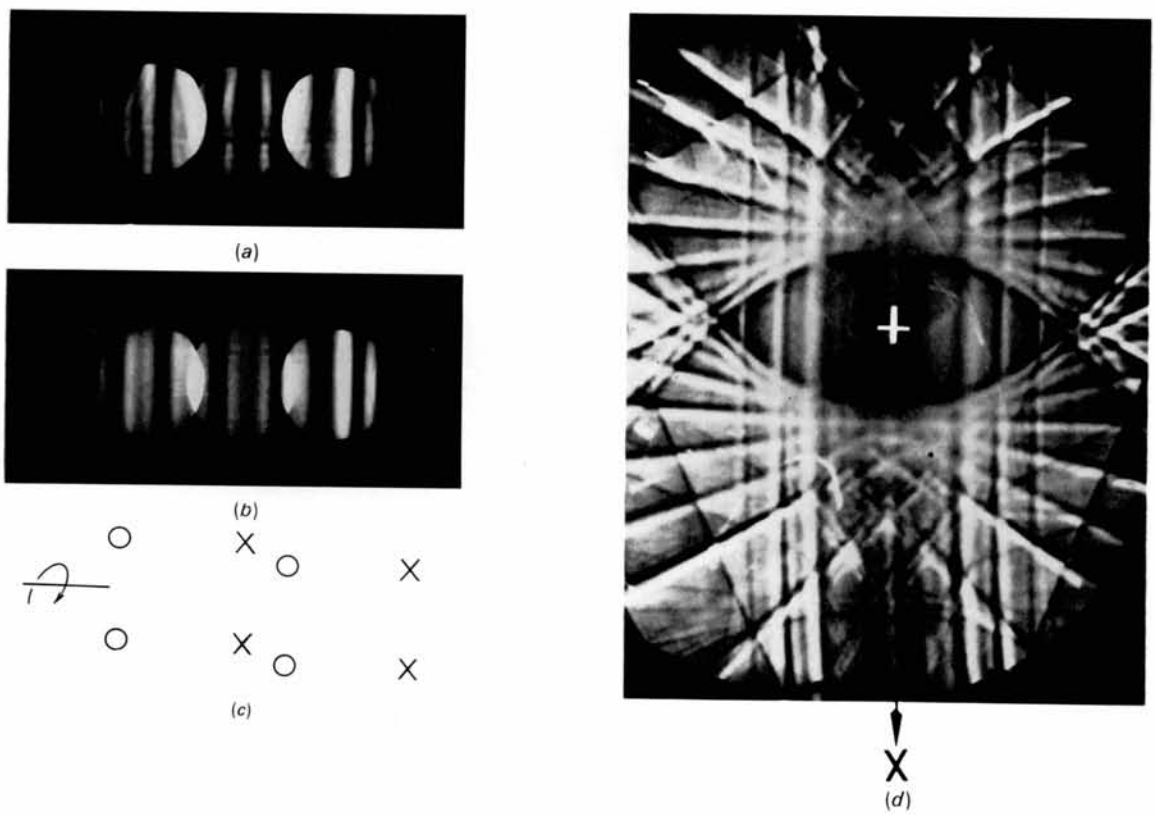

Fig. 7. Convergent beam patterns from region of [32$\bar{5}$0] zone axis of cadmium sulphide. (*a*) Kossel–Mollenstedt pattern of almost one-dimensional structure. The incident beam is placed centrally in the 0002 Kikuchi band, but removed from the [32$\bar{5}$0] zone-axis in a direction indicated by × in 7(*c*). The 000$\bar{2}$, 0000, 0002, beams are shown. (*b*) Similar pattern obtained for the [32$\bar{5}$0] zone-axis orientation, marked † in 7(*d*). (*c*) Projected structure in the [32$\bar{5}$0] direction, where the Cd (open circles) and S (crosses) atoms are directed as revealed by the calculation in Fig. 8(*c*). Rotation arrow indicates direction of the [21$\bar{3}$0] zone, as determined from indexing upper-layer lines in 7(*c*). (*d*) Kossel pattern, centred on the zone axis, indicating the regions from which the patterns of 7(*a*) and (*b*) were taken.

[*To face p.* 343

increase the sensitivity of the symmetry observations, as well as introducing increased coupling with the higher-layer reflexions.

The projection of Fig. 2 corresponds to the plane group *pm*, and has only a mirror-reflexion line. If we rotate the crystal into the [10$\bar{1}$0] projection, which has the symmetry of *pg*, with one glide-reflexion line, we generate forbidden 000*l* reflexions which display the on-axis dynamic extinction bands found previously (Goodman & Lehmpfuhl, 1964). Fig. 3 is taken from this projection with the beam symmetrical relative to the [000*l*]* axis. In addition to the forbidden bands, the diffraction pattern shows mirror symmetry about this axis. The exact zone axis orientation was avoided here, because of additional crossing extinction bands in this region complicating the pattern.

5. Calculations—applicability of systematic approximation

It was found previously (Goodman & Lehmpfuhl, 1967) that for structures sufficiently simple and composed of sufficiently light atoms, as for example magnesium oxide, it was possible to obtain accurate results with calculations based on systematic interactions only, provided the reflexions from a principal zone were not excited. Since cadmium sulphide has a much greater scattering potential and larger unit-cell dimensions than magnesium oxide the influence of the non-systematic interactions should be more important.

In order to obtain a pattern suitable for relatively simple calculation, the crystal was rotated about the *c* axis to a setting far from the zone axis, where a diffraction pattern of one-dimensional structure showing the symmetry properties occurring in one direction was obtained [Fig. 7(*a*)]. The crystal thickness here corresponded very nearly to an extinction length. A calculation was run which included only the 000*l* systematic interactions by the multi-slice method, as described in the previous work (Goodman & Lehmpfuhl, 1967). For this calculation 13 beams were used; scattering curves for Cd and S from Table 3.3.3.A of *International Tables for X-ray Crystallography* (1952) were used. Fig. 8(*a*) shows calculated results for the three main reflexions for a crystal thickness of 1249 Å. This thickness is in very approximate agreement with a determination from an isolated high-order reflexion using the simple kinematical relation. The main features of Fig. 7(*a*) are reproduced by the calculation. An outstanding deviation is that the minimum in the calculated 0000 distribution shows an appreciable intensity, whereas the experimental value is much nearer zero. In addition the agreement with calculation for the 0002, 000$\bar{2}$ distributions is not in itself sufficient to distinguish between the fitting at neighbouring extinction lengths. In proceeding from one extinction length to the next the behaviour of the 0002 and 000$\bar{2}$ reflexions are interchanged (see Fig. 7), so that determination of the absolute orientation of the crystal depends upon knowledge of the crystal thickness.

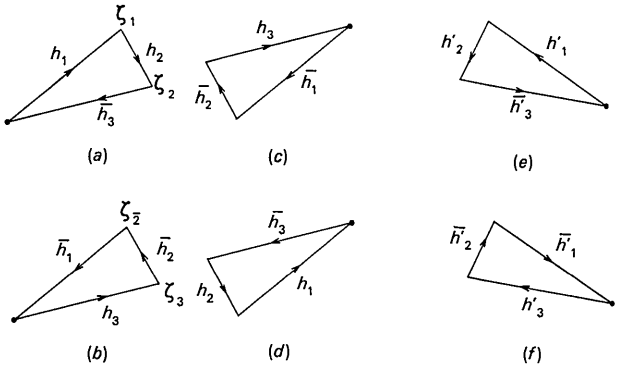

Fig. 6. Diagrams in reciprocal space for third-order scattering processes. The excitation errors ζ_1, ζ_2... of the text refer to the termination points in the diagrams of the h_1, h_2... vectors (corners of the triangle) (see also Gjønnes & Moodie, 1965). Diagrams (*a*), (*b*), (*c*) and (*d*) show processes occurring with the incident beam at equal inclinations on opposite sides of a zone axis, corresponding to what is observable in a convergent beam pattern. Equating of structure factors in the first and second pair of diagrams is then made with the proviso regarding higher-layer interactions discussed in §2. Diagrams (*e*), (*f*) show processes which are the processes (*a*), (*b*) mirrored across a principal (vertical) axis. Special relationships holding between F_{h_1} and $F_{h'_1}$, *etc.* due to symmetry across the axis, cause special symmetries in the central beam distribution (see text).

The closest non-systematic reflexions in the experiment were those from the [32$\bar{5}$0] zone. The crystal was turned to this orientation. The Kossel pattern from this region is shown in Fig. 7(*d*). A convergent beam pattern taken with the diffraction aperture in the centre of this region (marked by +) is shown in Fig. 7(*b*). The major change occurring between Figs. 7(*a*) and 7(*b*) can be described by the transfer of intensity to the centre of the 0000 distribution from regions in the diffracted distributions. Two-dimensional calculations by the multi-slice method were run which included the interactions from the [32$\bar{5}$0] zone, at first for the zone-axis setting, corresponding to Fig. 7(*b*) [+ position in Fig. 7(*d*)], and secondly for an orientation outside the zone as in Fig. 7(*a*) [× position outside Fig. 7(*c*)]. As shown by the crosses in Fig. 8(*a*), these calculations successfully describe the behaviour of the 0000 distribution at the central minimum, for Fig. 7(*a*) and (*b*). It was therefore clear that even for the orientation of Fig. 7(*a*) far from a strong zone, the pure systematic calculation based on only 000*l* interactions was inadequate, and a two-dimensional calculation was necessary to explain quantitatively the features of the distribution.

The difficulties of using the systematic approximation to describe diffraction from a structure exhibiting strong interaction may be best seen by examining the Pendellösung, or equal thickness fringes. Fig. 9 shows the calculation for symmetrical orientation (incident beam perpendicular to [0001]) including systematic 000*l* interactions. An oscillation of the diffraction asymmetry may be seen by comparing curves (*b*) and (*c*) in Fig. 9. By comparing the curve of Fig. 9(*a*) with

curve (1) of Fig. 10(*a*), which was made with two-dimensional calculations, the failure of the systematic approximation is exhibited. Firstly the curve of Fig. 9(*a*) never reaches zero, and further the cosinusoidal appearance of this curve is replaced in the full calculation [Fig. 10(*a*)] by a more damped oscillation. (In this latter respect the character is better shown by the two-dimensional phase-grating calculation which in the simple case of a cosine lattice gives for the zero-beam the zero-order Bessel function, than by the 2-beam or the systematic calculation for which the result is roughly cosinusoidal.) Moving to inside the zone-axis region (curve (2), Fig. 10) shortens the oscillation period, leading to the difference found between Figs. 7(*a*) and 7(*b*).

To examine the possibility of reducing the calculation in such cases of weak non-systematic interaction, a third type of calculation was run. For this a systematic calculation was made, using however scattering potentials 'corrected' for effects of non-systematic interaction. The 'corrected' 000*l* scattering potentials were derived by a two-dimensional phase-grating calculation for the [32$\bar{5}$0] orientation. In other words the multislice calculation was made one-dimensionally using only the ψ_l scattering amplitudes; but these were calculated by performing the summation

$$\psi_l = \sum_{x,z} \exp(i\sigma\Phi_{xz} \,.\, y) \,.\, \exp(i2\pi ly),$$

where Φ_{xz} is the two-dimensional projected potential

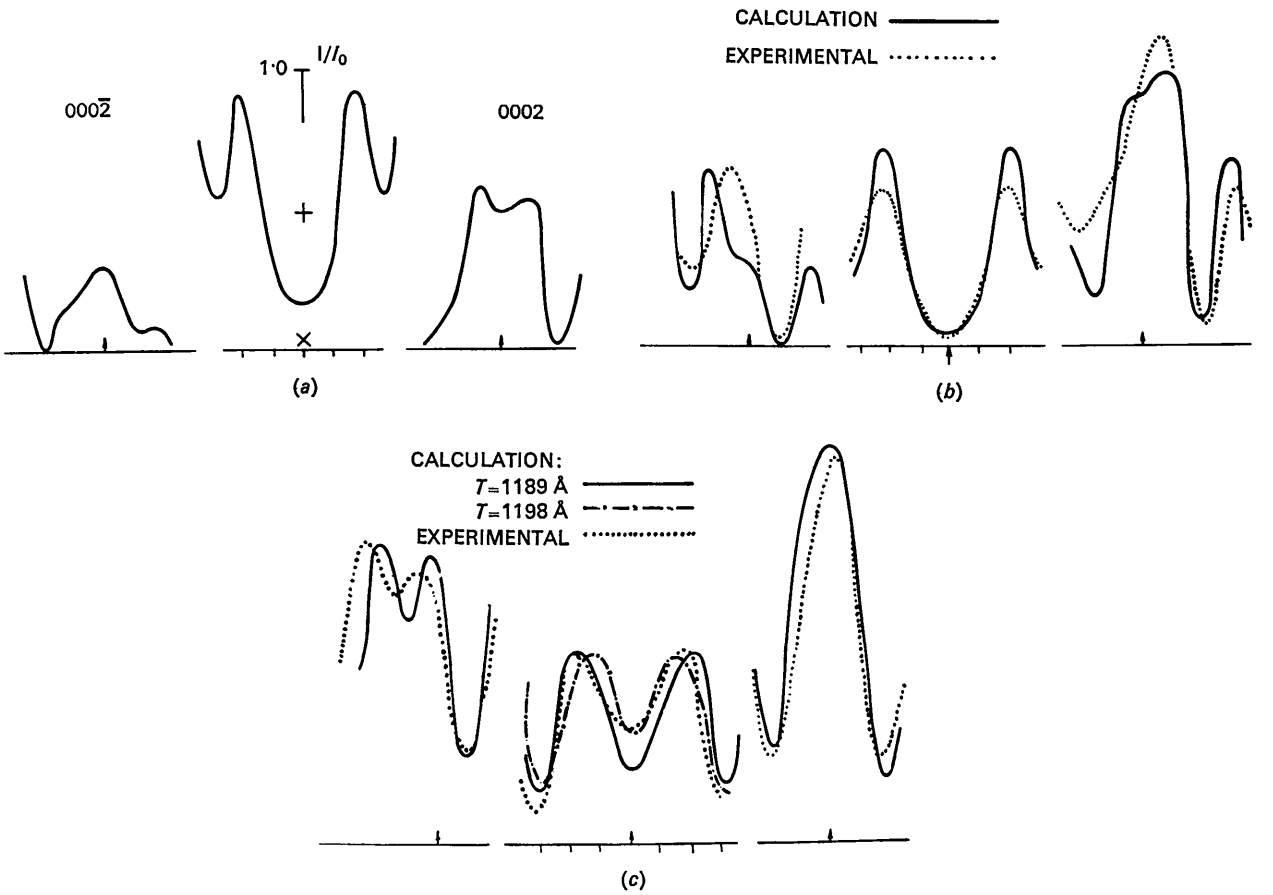

Fig. 8. Intensity distribution curves calculated by the multislice method (at 80 kV) of the 000$\bar{2}$, 0000, 0002 (from the left) reflexions, and plotted about the central position over an angular range corresponding to that of Fig. 7(*a*) and (*b*). One division on the horizontal scale corresponds to the angle ($\theta_{0002}/4$), where $\theta_{0002} = \lambda/2d_{0002}$. (*a*) Calculated for only systematic interactions between 000*l* reflexions, including 13 beams ($T = 1250$ Å). Added to the central curve are crosses showing values obtained for the central orientation by full two-dimensional calculation. The lower, diagonal cross corresponds to the orientation of Fig. 7(*a*) and the upper cross to that of Fig. 7(*b*). (*b*) Systematic calculation for 13 beams, using 'corrected' scattering potentials ($T = 1255$ Å), together with experimental curve obtained by scanning Fig. 7(*a*) with a vertical slit. Main deviations between experiment and calculation occur where interference from extra reflexions can be seen in the pattern. Experimental curves have an arbitrary intensity scale, and an arbitrary smooth background has been subtracted. (*c*) Full two-dimensional calculation for 117 beams for the angular distribution about the [32$\bar{5}$0] zone axis [corresponding to Fig. 7(*b*)], together with the experimental curve obtained from Fig. 7(*b*). Most features of the experimental curve are reproduced by this calculation. Probable reasons for discrepancies remaining between experiment and calculation are given in the text.

of the structure projected through a distance y (Cowley & Moodie, 1957), rather than taking

$$\psi_l = \sum_z \exp(i\sigma\Phi_z \,.\, y) \,.\, \exp(i2\pi lz),$$

where

$$\Phi_z = \frac{1}{a}\int_0^a \Phi_{xz} \,.\, dx,$$

which excludes all interactions from non-systematic reflexions. The results obtained show reasonable agreement with the intensities outside the zone [Fig. 7(*a*)], though not with those inside [Fig. 7(*b*)]. This is not surprising since the condition which such an approximation implies is that the amplitudes of the non-systematic reflexions are significant only for very thin crystals, for which the phase-grating approximation is valid, a condition which can only hold for crystal orientations sufficiently far from the zone. The thickness curve obtained by this method is almost identical with the full calculation for outside the zone (compare curves (1) and (3) of Fig. 10). Considering the enormous saving in calculation time involved, this is obviously a useful approximation to apply where neighbouring weak zones are present.

An angular distribution obtained by this method for a crystal thickness of 1255 Å shows rough agreement with the experimental curve obtained from Fig. 7(*a*) [Fig. 8(*b*)]. Regions of disagreement can be seen to occur particularly where the diffraction pattern of Fig. 7(*a*) shows interference from crossing non-systematic lines. Full two-dimensional calculation for this pattern was not carried out, since it appeared that such small deviations from one-dimensional character would make a more accurate comparison with calculation very difficult.

On the other hand, the intensity distributions *within* the zone [Fig. 7(*b*)] appeared much more one-dimensional in character. Therefore, it was practical to obtain reliable experimental curves, using the normal microphotometer method of scanning the pattern with a

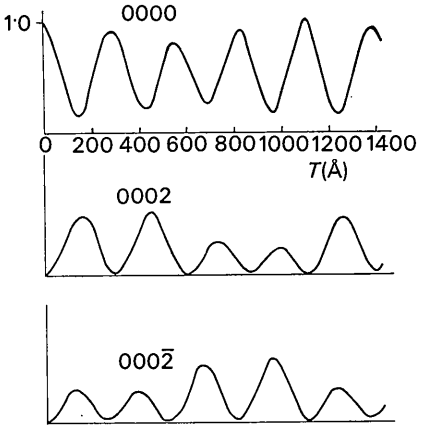

Fig. 9. Results, for the 0000, 0002, and 000$\bar{2}$ reflexion intensities, from a calculation for systematic interaction of 13 {000l} reflexions (E=80 kV).

vertical slit. The result thus obtained is shown together with a full two-dimensional calculation, for crystal thicknesses of 1189 and 1198 Å in Fig. 8(*c*). The absence of intensity change with tilts about the [0001] axis [*i.e.* parallel to the intensity stripes in Fig. 7(*b*)] can be understood by considering the main off-axis reflexions contributing to the zone-axis interaction, $2\bar{3}10$ and $\bar{2}3\bar{1}0$. Inside the zone region the excitation errors $\zeta 2\bar{3}10$ and $\zeta\bar{2}3\bar{1}0$ are both negative and therefore cause in-phase additions to the 'effective' 000l potentials (using the concept of weak-beam addition-potentials as derived by Bethe, 1928). Furthermore by rotating about the [0001] axis these ζ's change, one increasing as the other decreases so that the total correction remains fairly constant. If we pass just outside the zone region, however, one ζ becomes positive so that the two addition potentials are out of phase. The correcting potential then rapidly becomes a subtraction term, with consequent lengthening of the Pendellösung period. The phenomenon is related to the well-known appearance of Kikuchi bands (Shinohara, 1932), although here we have a crossing of two bands. It follows from this discussion, and from the form of the results in Fig. 8(*b*), that there should be a systematic approximation to the n-beam calculation also for this region using corrected potentials (analogous to addition-potentials), but at present there is no obvious way for obtaining the corrected potentials.

The agreement between experiment and calculation as shown in Fig. 8(*c*) is now quite good, and allows a sensitive estimate of crystal thickness to be made. The zero beam distribution shows a fit between 1189 Å and 1198 Å (125 and 126 slices) which agrees with a crystal thickness of 109 unit cells, with the c spacing 10·94 Å of this orientation (here the slice thickness and c spacing were not equivalent), which would represent the true thickness if we could assume that the structure potentials used for calculation were sufficiently accurate. However a difference between the thickness values from Fig. 8(*b*) and (*c*) probably indicates error in these potentials. Discrepancies remaining between the two curves can be understood from the following considerations:

(1) Assumption of a uniform intensity along the band inside the zone is only approximately justified.
(2) Scattering potentials for Cd and S used may not be sufficiently accurate.
(3) The diffuse (Kikuchi) pattern which occurs as a background to the diffraction pattern is included in the measured curve, though not in the calculation.
(4) Upper-layer interactions have not been correctly taken into account.
(5) The calculation was made without considering absorption.

These points could be taken into account in a more complete investigation, but further refinement was not undertaken at this stage.

An interesting point arises concerning the diffuse pattern (3). As may be seen in Fig. 8(*c*), there is some asymmetry in the experimental zero beam pattern. This cannot be due to the asymmetric upper layers which exist for this projection, since in this case these can only cause asymmetry perpendicular to [000*l*]*. Moodie (1967) showed that the symmetry of the zero beam is maintained even after introducing phenomenological absorption into the structure potentials. However, the proof will not be valid for diffuse scattering since this has a finite scattering angle, so that the diffuse pattern surrounding the zero beam can have an asymmetry due to the breakdown of Friedel's law.

The numerical analysis above has determined the absolute orientation of the crystal giving rise to Fig. 7, although this would not have been possible from simple inspection of the main beams except for very thin crystals. An oscillation of the diffraction asymmetry occurs between the 0002 and $000\bar{2}$ beams with thickness, although it can be seen that *on the average* the 0002 beam [Fig. 10(*b*)] is the stronger. Results from Fig. 9(*c*) show that for Fig. 7 the Cd → S axis is directed as shown in the structure diagram, Fig. 7(*c*). Further, indexing of the upper-layer lines of 7(*c*) determines the direction of rotation of the crystal from the nearest principle zone [arrow of Fig. 7(*c*)].

6. Summary

The diffraction pattern of cadmium sulphide has been analysed in a preliminary exercise, to explore the possibilities of systematic analysis in determining elements of symmetry from the electron diffraction pattern. In particular, where the stability of the specimen permits examination, detection of presence or absence of a centre of symmetry may be a useful adjunct to an X-ray analysis, since this symmetry is not revealed directly by kinematic X-ray intensities. Also the possibility clearly exists of fairly accurate determination of an asymmetric component of potential distribution, using *n*-beam calculations. Such discussion applies to perfect crystals. For disordered crystals further consideration is necessary, since the dynamic symmetry refers to the symmetry of the whole crystal.

In conclusion the authors wish to thank Mr A.F. Moodie for his continued interest and for first pointing out the reason for the special symmetry of the zero-order beam distribution, and Dr A.W.S. Johnson for his guidance in editing the manuscript.

References

BETHE, H. (1928). *Ann. Phys. Lpz.* **87**, 55.
COCKAYNE, D. H. J., GOODMAN, P., MILLS, J. C. & MOODIE, A. F. (1967). *Rev. Sci. Instrum.* **38**.
COWLEY, J. M. & MOODIE, A. F. (1957). *Acta Cryst.* **10**, 609.
COWLEY, J. M. & MOODIE, A. F. (1959). *Acta Cryst.* **12**, 360.
COWLEY, J. M. & MOODIE, A. F. (1962). *J. Phys. Soc. Japan*, **17**, B-II, 86.
COWLEY, J. M., MOODIE, A. F., MIYAKE, S., TAKAGI, S. & FUJIMOTO, F. (1961). *Acta Cryst.* **14**, 87.
FRIEDEL, M. G. (1913). *C.r. Acad. Sci. Paris*, **157**, 1533.

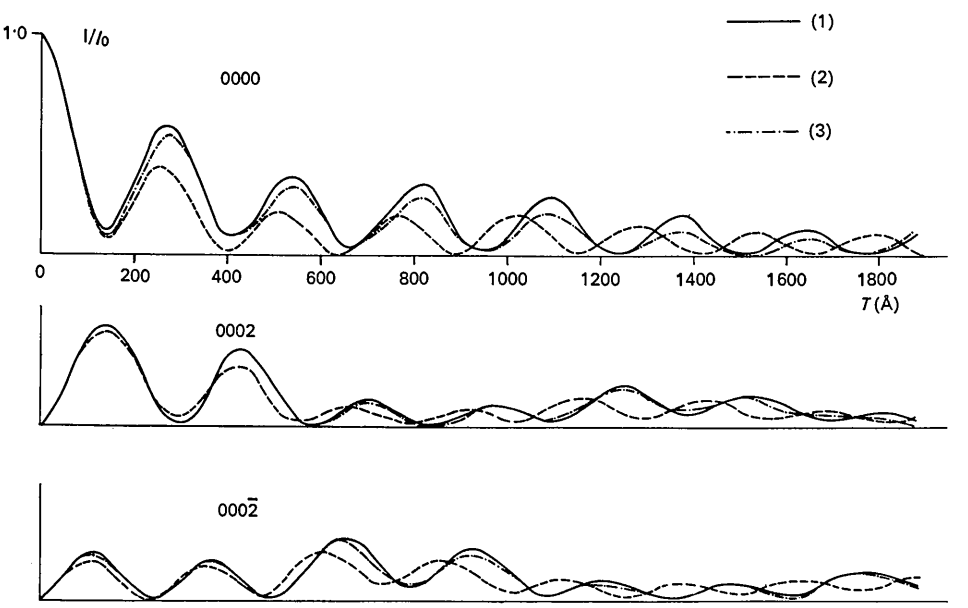

Fig. 10. Intensities calculated as a function of thickness for reflexions shown in Fig. 9, but taking into account two-dimensional interactions, as was done for Fig. 8(*b*) and (*c*). Curve (1): Two-dimensional multi-slice calculation. Incident beam in the (0001) plane, but inclined at approximately 3° to the [32$\bar{5}$0] zone-axis. [× in Fig. 7(*c*).] Curve (2): The same calculation at orientation of zone axis. [† in Fig. 7(*c*).] Curve (3): Systematic multi-slice calculation, by the same procedure as in Fig. 9, but using 'corrected' scattering potentials obtained by the phase-grating calculation for the zone-axis projection. A close correlation is shown with curve (1), apart from a heavier damping.

FUJIMOTO, F. (1959). *J. Phys. Soc. Japan*, **14**, 1958.
FUJIWARA, K. (1959). *J. Phys. Soc. Japan*, **14**, 1513.
GJØNNES, J. & MOODIE, A. F. (1965). *Acta Cryst.* **19**, 65.
GOODMAN, P. & LEHMPFUHL, G. (1964). *Z. Naturforsch.* **19a**, 818.
GOODMAN, P. & LEHMPFUHL, G. (1965). *Z. Naturforsch.* **20a**, 110.
GOODMAN, P. & LEHMPFUHL, G. (1967). *Acta Cryst.* **22**, 14.
IBERS, J. A. & HOERNI, J. A. (1954). *Acta Cryst.* **7**, 405.
International Tables for X-ray Crystallography (1952). Vol. I. Birmingham: Kynoch Press.
KAMBE, K. (1957*a*). *J. Phys. Soc. Japan*, **12**, 13.
KAMBE, K. (1957*b*). *J. Phys. Soc. Japan*, **12**, 25.
KOHRA, K. (1954). *J. Phys. Soc. Japan*, **9**, 690.
LAUE, M. VON (1948). *Materiewellen und Ihre Interferenzen*, p. 257. Leipzig: Akad. Verl.
MIYAKE, S. & UYEDA, R. (1950). *Acta Cryst.* **3**, 314.
MIYAKE, S. & UYEDA, R. (1955). *Acta Cryst.* **8**, 335.
MOODIE, A. F. (1968). To be published.
SHINOHARA, K. (1932). *Sci. Pap. Inst. phys. chem. Res. Tokyo*, **18**, 223.
TANAKA, M. & HONJO, G. (1964). *J. Phys. Soc. Japan*, **19**, 954.
THIESSEN, P. A. & MOLIÈRE, K. (1939). *Ann. Physik*, **34**, 449.

Acta Cryst. (1968). A**24**, 347

The Derivation of a Set of Scattering Factors from X-ray or Neutron-Diffraction Structure-Factor Measurements

BY C. WILKINSON AND P. J. BROWN
Crystallographic Laboratory, Cavendish Laboratory, Cambridge, England

(*Received* 14 *June* 1967)

Scattering factors for the atoms in a structure may be evaluated as functions of the scattering vector **s** when a complete set of two- or three-dimensional structure factor measurements is available.

Introduction

Recently (*e.g.* Dawson, 1967*a*,*b*) there has been interest in the variation of the atomic scattering factor with the orientation of the scattering vector. A method for the determination of a set of spherically averaged form factors $f_j(|\mathbf{s}|)$ from a zone of structure factors has been described by Brown & Wilkinson (1965). The purpose of the present note is to show that a similar calculation may be used to determine from a zone or sphere of observed structure factors of known phase the scattering factors $f_j(\mathbf{s})$ as functions of the scattering vector $\mathbf{s}(=\mathbf{d}^*)$.

Method of calculation

The electron-density distribution which is obtained by Fourier inversion of a three-dimensional set of structure factors is given by

$$\varrho(r_j)=(1/V)\sum_{\mathbf{k}} F(\mathbf{k})\exp(2\pi i\mathbf{r}_j\,.\,\mathbf{k})\exp(2\pi i\mathbf{Q}_j\,.\,\mathbf{k})$$

where $\mathbf{r}_j$ is the radius vector from the centre of the jth atom which is vector distance $\mathbf{Q}_j$ from the origin of the structure factors $F(\mathbf{k})$, V is the unit-cell volume and $\mathbf{k}$ is the scattering vector.

The scattering factor for this atom is defined to be

$$f_j(\mathbf{s})=\int\varrho(\mathbf{r}_j)\exp(2\pi i\mathbf{r}_j\,.\,\mathbf{s})d\tau_j\,,$$

the integration being over the whole 'volume' of the atom. Thus

$$f_j(\mathbf{s})=\int(1/V)\sum_{\mathbf{k}}\{F'(\mathbf{k})\exp(2\pi i\mathbf{r}_j\,.\,\mathbf{k})\exp(2\pi i\mathbf{r}_j\,.\,\mathbf{s})\}d\tau_j$$
$$=(1/V)\sum_{\mathbf{k}}F'(\mathbf{k})\int\exp[2\pi i\mathbf{r}_j\,.\,(\mathbf{s}+\mathbf{k})]d\tau_j\,,$$

where $F'(\mathbf{k})$ has been written for $F(\mathbf{k})\exp(2\pi i\mathbf{Q}_j\,.\,\mathbf{k})$.

Let α be the angle between $(\mathbf{s}+\mathbf{k})$ and $\mathbf{r}$. Then

$$f_j(\mathbf{s})=(1/V)\sum_{\mathbf{k}}\left\{F'(\mathbf{k})\int_{r_j=0}^{R_0}\int_{\alpha=0}^{\pi}\exp(2\pi i r_j|\mathbf{s}+\mathbf{k}|\cos\alpha)2\pi r^2\sin\alpha d\alpha dr\right\}$$
$$=\frac{1}{2\pi^2V}\sum_{\mathbf{k}}\left\{\frac{F'(\mathbf{k})\{\sin(2\pi R_0|\mathbf{s}+\mathbf{k}|)-2\pi R_0|\mathbf{s}+\mathbf{k}|\cos(2\pi R_0|\mathbf{s}+\mathbf{k}|)\}}{|\mathbf{s}+\mathbf{k}|^3}\right\},$$

where R_0 is the atomic 'radius'.

A similar expression can be derived for the extraction of a scattering factor from a zone of reflexions. If **s** is any scattering vector in the zone then

$$f_j(\mathbf{s})=R_0/A\sum_{\mathbf{k}}\left\{\frac{F'(\mathbf{k})J_1(2\pi|\mathbf{s}+\mathbf{k}|R_0)}{|\mathbf{s}+\mathbf{k}|}\right\}.$$

J_1 is the first order Bessel function and A the area of the unit cell in projection.

Numerical calculation of form factors

The calculations have been programmed for the TITAN computer and have been tested with 'prepared' data generated for an imaginary structure having Mn^{3+} ions with one 3*d* electron placed on a primitive cubic lattice of cell side 3 Å. The single 3*d* electron was given